Journal of Fluorescence, Vol. 12, Nos. 3/4, December 2002 (© 2002)

Study of Solid Transparent Nanocomposite Organic/Inorganic Matrices and Thin Films by Time-Resolved Fluorescence Techniques

Panagiotis Lianos[1]

Received March 21, 2002; revised June 10, 2002; accepted June 14, 2002

This work focuses on the study of nanocomposite organic/inorganic materials, particularly, those made by the sol-gel method, by using time-resolved fluorescence techniques. A model of stretched exponentials is presented and used to fit fluorescence (luminescence) decay profiles for fluorescence quenching reactions obtained by energy-transfer or by diffusion or both. Various types of information on both bulk and thin-film nanocomposite materials can be obtained by such analysis: for example, determination of the percolation threshold for the organic subphase, localization or mobility of incorporated molecular species, and extraction of structural parameters.

KEY WORDS: Fluorescence; probling; sol-gel; nanocomposites.

INTRODUCTION

Time-resolved fluorescence (or more generally, luminescence) spectroscopy has been established as the most efficient and popular technique for the study of organized molecular assemblies, such as micelles, microemulsions, lipid vesicles, polymers, etc., in colloidal solutions or wet gels. Time-resolved fluorescence has not received equivalent attention by materials scientists. The reason is that in the case of materials, which are usually studied and used in the solid state, researchers rely on imaging techniques, such as electronic microscopy, X-ray diffraction, etc. to characterize their materials. However, imaging techniques have their limits. Electronic microscopy, X-ray diffraction, and all the equivalent modern techniques rely on the existence of short- or long-range order [1–6] to obtain detectable signals and sufficient contrast to satisfactorily image the material's structure. Not all materials are endowed with such convenient properties. In particular, most of organic/inorganic nanocomposite gels are composed of interpenetrating subphases mixed in the nanoscale [7] so that microscopy or X-ray diffraction can provide only limited structural information or no information at all. In that case, only spectroscopy can offer the necessary tool to decipher the structure of these materials. Indeed, NMR and IR spectroscopy have been systematically employed in the study of such systems [7–10]. Steady-state luminescence spectroscopy has also been used, mainly to monitor gel evolution, particularly in sol-gel processes [10–14]. Both added probes [11] and intrinsic luminescence [14] have served in the study of both pure oxide or hybrid orgnanic/inorganic materials [10–14].

Fewer are the cases in which time-resolved luminescence analysis has been used for structural characterization of nanocomposite organic/inorganic materials. To properly map the structure of a material by luminescence techniques, it is necessary to analyze the geometry of the interaction between two species, one of which is excited and can emit light and a second one that can interact with excited species and quench their luminescence. The efficiency of such an interaction can by proper analysis

[1] University of Patras, Engineering Science Department, 26500, Patras, Greece. Tel.: 30-610997587. Fax: 30-610997803. e-mail: lianos@upatras.gr

1053-0509/02/1200-0303/0

provide information about the geometry of the distribution of the interacting species and, indirectly, about the geometry of the hosting environment. Time-resolved luminescence analysis is more efficient in providing such information than steady-state analysis, for several reasons: the related models of analysis are simpler and easier to deal with; time-resolved analysis provides information in a dynamic manner, whereas steady-state analysis gives only average values; and time-resolved analysis has higher resolution capacity and higher sensitivity in the mapping of the hosting environment. Nevertheless, in most cases the researcher relies on both steady-state and time-resolved data for a better mapping of the system. In the present work, we will present some of the techniques used to study nanocomposite organic/inorganic materials, made by the sol-gel process, by employing time-resolved luminescence analysis, emphasizing on our own work in this domain.

SOL-GEL PROCESS AND NANOCOMPOSITE ORGANIC/INORGANIC MATERIALS

Sol-gel is a chemical process that starts with a mixture of reagents making a transparent sol and ends up with a solid gel, and finally, after slow evaporation of volatile components, the result is a xerogel. Even though the term has a more general sense, it is usually employed to designate the hydrolysis of a metal alkoxide (including silicon alkoxides) and the subsequent inorganic polymerization (condensation) that leads to formation of the corresponding oxide [15,16]. The whole process is carried out at ambient or a slightly elevated temperature. The most extensively used reagents are silicon alkoxides, and compounds of several transition metals, such as Ti, Sn, Zn, or V, are also very popular [3,4,15–18]. One of the principal applications of the sol-gel process is the fabrication of transparent amorphous oxides doped with functional organic groups. Because sol-gel doping is done at ambient conditions or at slightly elevated temperatures, organic dopants can be preserved both in terms of composition and functionality. Thus, silica has been doped in a multitude of cases with organic substances ranging from laser dyes to proteins and other functional macromolecules [19–22]. It was, however, soon made clear that pure sol-gel matrices (in most cases, silica matrices) have serious drawbacks. The solubility of most organic substances, especially, hydrophobic ones, is limited in pure silica, causing migration, aggregation, and subsequent decrease of functionality. This is one main reason that research has turned to nanocomposite materials, made of two subphases mixed in the nanoscale, one organic and one inorganic. The inorganic subphase is the oxide network. The organic subphase aids solubilization and dispersion of functional dopants, while in some cases the functional dopant itself constitutes the organic subphase. A second main reason for seeking for nanocomposite materials is templating of mesoporous structures. This method, which is a vast field in materials research, uses organic mesophases in nanocomposite materials as templates to build porosity in oxide matrices. When the template is removed, either by calcination or by using appropriate solvents, it leaves behind a mesoporous structure, which can be designed to have a high degree of order [1–5].

Nanocomposite organic/inorganic materials are divided into two main categories: (1) materials in which the organic and the inorganic subphases make a simple mixture at the nanoscale; and (2) materials in which the two subphases are covalently linked. The materials of the first category can be easily made, and they can be chosen among a large variety of components. Typical substances making the organic subphase are surfactants, block copolymers or poly(alkyleneoxide) oligomers [1–7,22–31]. In the second category, the precursor introduced in the original sol is a hybrid composed of the functional organic group covalently linked with (usually) silicon alkoxide group(s). The sol-gel process leads to inorganic polymerization, providing a covalent linking with the organic subphase. Such materials are stable and have excellent mechanical and optical properties, and for this reason they are quite popular [13,14,32–41]. Both categories of these materials, which will be henceforth called by a single name “nanocomposite organic-inorganic materials,” are the subject of the present work.

TIME-RESOLVED FLUORESCENCE ANALYSIS BY STRETCHED EXPONENTIALS

Time-resolved analysis of fluorescence decay profiles by stretched exponentials has been known for a long time. Until the 1980s it was limited only to a particular model assigned to resonance energy transfer between an excited donor and a quencher-acceptor. Briefly, this model, which is found in any photophysics textbook [42], is described as follows. The efficiency of resonance energy transfer from excited donors to randomly distributed acceptors is given by:

$$k(r) = \frac{1}{\tau}\left(\frac{R_0}{r}\right)^6 \tag{1}$$

where k is the rate of energy transfer, τ is the decay time

of the donor in the absence of an acceptor, r is the distance between an excited donor and an acceptor, and R_0 is a characteristic distance, termed the Foerster distance, that is specific for a given donor–acceptor pair and corresponds to a transfer efficiency of 50% [42]. The exponent 6 of the power of distances R_0 and r corresponds to energy transfer by dipole–dipole interaction [43], which is the prevalent type of interaction in most cases. The energy transfer rate depends then on the distance between donors and acceptors. This fact offers a relationship between the geometry of the dispersion medium and the reaction rate. Thus, the analysis of the latter gives information on the structure of the former. When excitation of the donors is made by light pulses, which are short compared with the life time, τ, of the excited state, the energy transfer rate evolves with time, that is, it is time-dependent. Time dependence is a consequence of distance dependence, because the probability of interaction between close-lying species is higher than that of far-lying reacting species. The time-dependence of the reaction rate is reflected in the form of the fluorescence decay profile, which can be represented by the following generalized formula (cf. ref. [42]):

$$I(t) = I_0 \exp(-t/\tau) \exp(-Ct^{1/2}) \qquad (2)$$

where I is the fluorescence intensity and C is a constant, the meaning of which will be detailed below. The non-integer power of time (hence the name stretched exponential) is a consequence of the distance dependence of the energy transfer rate of Eq. (1). More information will be provided below.

The model of Eq. (2) was successfully employed to study energy transfer in solutions, where the randomness of the donor and acceptor distribution is guaranteed. However, problems were encountered when the model was used in solid media, where fitting of Eq. (2) to fluorescence decay profiles gave non-integer powers of t smaller than 1/2. The explanation of this finding was made possible with the advent of the fractal theory and the understanding of fractal geometry. It was thus understood that in a solid medium, particularly a non-isotropic or a composite medium with distinct subphases, the distribution of the reacting species is restricted. This restriction, or low dimensionality of the reaction medium, is reflected on the power of time within the stretched exponential of Eq. (2). In fact, as has been found, the most general form of Eq. (2) that applies also to restricted environments is given by the following equation (cf. refs. [43–45]):

$$I(t) = I_0 \exp(-t/\tau) \exp(-Ct^f) \quad 0 < f < 1, f = d/6 \qquad (3)$$

where d is the dimensionality of the reactant distribution, which, in principle, coincides with the dimensionality of the dispersion medium. Eq. (3) allows for f, the power of time, to get any value between 0 and 1/2, for restricted geometries where d ranges between 0 and 3. Eq. (3) manages to describe decay profiles for direct energy transfer between immobile reactants. It still fails to fit decay profiles for energy migration or transfer between mobile reactants. Fortunately, appropriate models have been developed also for these cases [45]. In the course of these studies we have found that the generalized stretched exponential models that describe these phenomena include not only energy transfer processes but any type of bimolecular interaction in a restricted medium. For this reason, we present a general model and the theory underlying it in the next paragraph.

Fluorescence quenching in media where migration is allowed can generally be analyzed into two parts. One part is energy exchange between the excited and the quenching species. Energy exchange, in the most general sense of the term, includes all kinds of electrical and magnetic interactions, whether they are dipolar, multipolar, exciton, or electron transfer. What makes resonance energy or electron transfer be distinguished from other processes is that the reaction radii in that case can be large. We can then safely approximate the rates of any type of excited state interaction by an inverse power law of distance, $k \approx 1/r_s$, that is, similar to the one given by Eq. (1). In this sense, resonance energy transfer by dipole-dipole interaction will correspond to relatively low s-values (e.g., $s = 6$). Collisional quenching or, generally, contact quenching will correspond to large s-values (multipolar interactions) [43]. The second part of fluorescence quenching is a diffusion-controlled process. We may represent diffusional motion in the reaction medium by a random walk on solubilization sites. To derive a decay model we can use a cumulant expansion, introduced by Blumen, Klafter, and Zumofen [45,46] to describe energy migration in lattices with spatial disorder. In terms of cumulants the decay law becomes:

$$I(t) \approx \exp\left[\frac{\kappa_i(t)(-\lambda)^i}{i!}\right] \qquad (4)$$

where κ_i are the cumulants, $\lambda = -\ln(1 - p)$, and p is the occupation probability of lattice sites by traps. In our case, p can be the ratio of the number of quenchers by the number of solubilization sites, that is, the quencher concentration. It is known that for any distribution of reaction probabilities and for a given value t of time, $\kappa_1(t)$ is equal to the mean, and $\kappa_2(t)$ is equal to the variance. In random walk, the reaction rate is determined by the number of distinct sites $S(t)$ visited by the random walker within time t. Then $\kappa_1(t)$ is proportional to the mean of

$S(t)$ and $\kappa_2(t)$ to its variance. Higher-order cumulants are more complicated expressions also involving $S(t)$. We should also note that in regular lattices $S(t) \approx$ t but in lattices with spatial disorder $S(t) \approx t^f$, where $0 < f < 1$, because in that case, repeated visits to the same sites will make the number of distinct sites visited smaller that the number of steps. By looking at the form of Eq. (4), it is obvious that the successive cumulants introduce successive powers of t into the decay law with exponents been integral multiples of f. Therefore the decay law for diffusion-controlled collisional quenching can be written as [47,48]:

$$I(\mathrm{t}) = I_0 \exp(-t/\tau) \exp(-C_1 t^f + C_2 t^{2f} - C_3 t^{3f} + \ldots\ldots)$$
$$0 < f < 1 \qquad (5)$$

where f, C_1, C_2, C_3, . . . are constants and τ is, as already said, the decay time in the absence of quenchers. From Eq. (4), it is also obvious that the Cs are related to λ and p, that is, to quencher concentration. This simplified decay law is now useful for practical applications if an important question is answered: are the Cs related with each other or are they independent? Inspection of Eq. (4) reduces the question to whether the cumulants κ_i are correlated. There are discrete distributions, such as Poisson or binomial distribution, where the κs are given by specific relations. In the most common case, the normal (Gaussian) distribution, the first cummulant is equal to the mean and the second to the variance, which are not related, while all higher-order terms are 0. Fluorescence decay profiles recorded by the photon counting technique, thus containing noisy data, correspond to Gaussian distribution of data. Such profiles should be described by the form of Eq. (5) with C_1 and $C_2 \neq 0$ and all the higher-order constants equal to 0. This conclusion has been experimentally proven on several occasions [47]. Both C_1 and C_2 depend on quencher concentration, but they are also influenced by dispersion, defined by the physical system itself. Therefore, they are not correlated. If the distribution of the reaction probabilities is not normal, then C_3 and higher-order terms will be different from 0 and the Cs will be correlated.

The decay law of Eq. (5), which is a combination of stretched exponentials, introduces a specific dependence on geometry, through the value of f. Low f corresponds to spatially restricted reactions, whereas $f = 1$ corresponds to the classical case of completely non restricted reaction. The importance of higher-order terms in the power series of Eq. (5) increases with spatial restriction. Experience has shown that noisy data can be perfectly fitted even with only one term of the series being different from zero (i.e., $C_1 \neq 0$, $C_2 = 0$). In other cases both C_1 and C_2 must be $\neq 0$.

By exploiting the form of Eq. (5), a mathematical relation for the first-order reaction rate can be obtained by simple differentiation:

$$K(t) = fC_1 t^{f-1} - 2fC_2 t^{2f-1} + \ldots\ldots \qquad (6)$$

which is, of course, time-dependent.

When quenching is carried out by resonance energy transfer between moving partners, we can conclude, by inspection of Eqs. (3) and (5), that there will be two contributions of the form t^n, $0 < \mathrm{n} < 1$, that is, $Ct^{d/s} + C_1 t^f$. Experience shows that it is very hard to distinguish $Ct^{d/s}$ from $C_1 t^f$ by fitting procedures. Therefore, experimental decay profiles in cases of energy transfer to moving acceptors can still be described by the stretched exponentials of Eq. (5). Eqs. (2) and (3) would then be special cases of Eq. (5). f values are higher in the case in which both transfer and diffusion occur simultaneously [30] so that f can increase above the limited value of 1/2 (Eq. (2)). When motion of the reacting species can be excluded, resonance energy transfer in restricted media will be simply described by Eq. (3). In that case the constant C can be analyzed into a detailed expression [49,50] that can offer valuable information on the structure of the system under study. Indeed,

$$C = pF(R_0/\alpha)^d g\Gamma(1 - f) \quad f = d/s \quad s = 6 \qquad (7)$$

where p is the occupation probability of available solubilization sites by acceptors, F is a shape factor that depends on the structure of the reaction domain, g is an orientation factor that depends on the mutual donor acceptor orientation, α is a unit size in the reaction domain, R_0 is the critical reaction radius (Foerster distance), and d the dimensionality [27]. Applications of these models will be shown in the next section.

APPLICATIONS TO THE STUDY OF NANOCOMPOSITE ORGANIC/INORGANIC MATERIALS

This section presents applications of the above time-resolved fluorescence models to the study of a few characteristic nanocomposite materials.

Determination of the Percolation Threshold

If we search for an "ideal" case for applying the fluorescence decay model of Eq. (5) this is determination of the percolation threshold. Let us consider the case of

a nanocomposite organic/inorganic material where the organic subphase makes the minority component. We want to search for the conditions in which the organic subphase will form a percolating cluster. If we use two interacting species, such as a fluorophore and a quencher, associated with the organic subphase and follow the kinetics of their interaction it is possible to relate kinetics with the geometrical characteristics of the hosting subphase. Indeed, as it has been explained in the previous section, the exponent *f* of time in Eqs. (3), (5), and (6) is proportional to the dimensionality of the reaction domain. By assuming that the interaction proceeds by random walk, it has been shown that the value of *f* is equal to 2/3 at the percolation threshold [51,52]. However, imaging a percolation cluster by indirect methods, such as fluorescence quenching, is a rather tricky affair. Probing of the reaction domain will depend on the time scale of observation. In the case of fluorescence quenching, it will depend on the lifetime of the excited state of the fluorophore. For this reason it is necessary to employ both time-resolved fluorescence and other supporting techniques to obtain exploitable results. In our case, we have searched for a nanocomposite ionic conductor made of silica and poly-(ethyleneglycol)-200 (hereafter called PEG). Silica makes the gelling factor of the material while PEG is the ion conducting organic subphase [53]. It was then necessary to apply the nanocomposite material as a thin film, in a sandwich configuration between two electrodes [31]. The quality of the film increased with the percentage of silica; however, conductivity increased with the percentage of PEG as it can be seen in Fig. 1. It was then necessary to define a compromising composition that would give sufficient conductivity with maximum possible silica content in order to obtain quality films. The answer was provided by analysis of the luminescence decay profiles of $Ru(bpy)_3^{2+}$ [tris(2,2′-bipyridine)ruthenium dichloride hexahydrate] in the presence of MV^{2+} [methylviologen], which acts as quencher of $Ru(bpy)_3^{2+}$ luminescence [31], both incorporated in the nanocomposite film. Both cations are associated with the organic (PEG) subphase, and they are thus appropriate to probe it. Fitting of Eq. (5) to the luminescence decay profiles [31] gave the corresponding values of *f*, which are shown in Fig. 2. The data of Fig. 2 reveal that the percolation threshold ($f = 2/3$) is obtained for PEG content lying around 8% w/w. For higher PEG content the *f* value tends to a plateau. Indeed, maximum performance of a cell made with this material was realized at a composition of the nanocomposite material just above the percolation threshold [31], where the conductivity reaches important values, as seen in Fig. 1.

Probing Domain Polarity and Mobility in Surfactant/Silica Nanocomposites

Sol-gel nanocomposites made of silica and surfactant are composed of a polar inorganic nanophase (silica

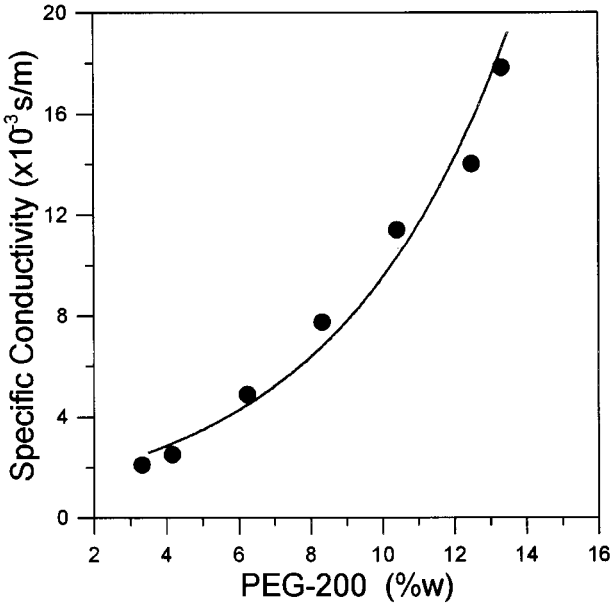

Fig. 1. Steady-state specific conductivity of an I_3^-/I^- electrolyte (0.5 M IK, 0.05 M I_2) vs. PEG weight percent in PEG/silica nanocomposites made by the sol-gel method. T = 25°C.

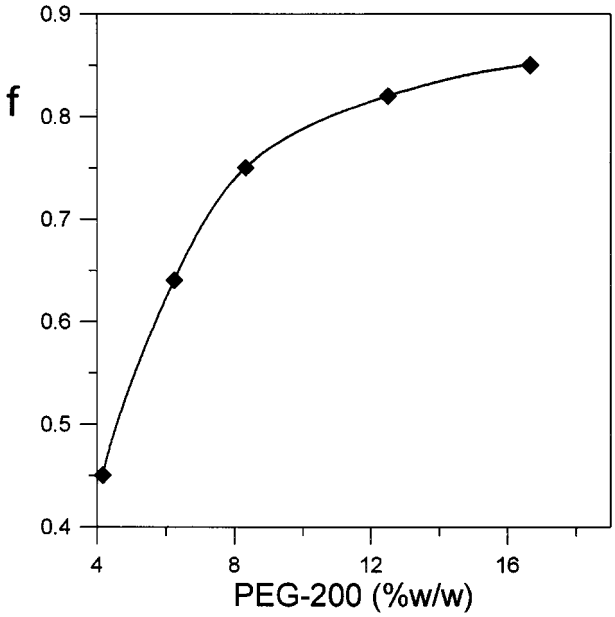

Fig. 2. *f*-values vs. PEG weight percent at 20°C, for a nanocomposite film made of PEG/silica and containing 1 m*M* $Ru(bpy)_3^{2+}$ and 20 m*M* MV^{2+} (cf. Ref. [31]).

network) and of a surfactant nanophase. The latter is a result of fusion of micelles found in the precursor sol [30]. The surfactant nanophase may form a percolating cluster if sufficient amount of surfactant is introduced in the nanocomposite material. In any case, the surfactant nanophase possesses some degree of molecular organization providing a hydrophobic core and a polar-hydrophobic interface with the embedding silica. Hydrophobic probes, such as pyrene, are immobilized in porous silica in the absence of surfactant. On the contrary, in the presence of surfactant, pyrene is solubilized in the surfactant subphase, where it is permitted to form diffusion-controlled excimers. The kinetics of excimer formation can be studied by analysis of monomer pyrene fluorescence decay profiles in the presence of excimers by using the model of Eq. (5). An example is given by the data of Table I, which refer to a material made of silica and cetyltrimethylammoniumbromide (CTAB). It is seen that the value of *f* for pyrene excimer formation in that system is around 0.7 and it is, practically, independent of pyrene concentration. This value indicates diffusion-controlled reaction in a percolating cluster (because f $>$ 2/3, cf. previous paragraph). Pyrene was also introduced in the same material at lower concentration, so that excimer formation was excluded, and its fluorescence was quenched by another hydrophobic species, C153 (coumarin-153). Quenching in that case is done by resonance energy transfer from excited pyrene to C153 [27,30,54]. The results of the analysis of the fluorescence decay profiles by Eq. (5) in that case are also shown in Table I. It is interesting to find that the *f* value is practically the same, that is, around 0.7, also in the present case as it was in the case of pyrene excimer formation. This results indicates the generality and the efficiency of the applied analysis model. In the case then of pyrene-C153 interaction, quenching is also controlled by diffusion, so that *f* is larger than the value of 0.5 applying to the classical case of Eq. (2) (see previous section). The same as above nanocomposite material was also studied by using a hydrophilic probe-and-quencher couple: $Ru(bpy)_3^{2+}$ and MV^{2+}, both introduced in the previous paragraph. These molecules are completely expelled from the surfactant subphase, not only because they are hydrophilic but also because they are positively charged, as the surfactant head groups of CTAB. They then, in principle, reside in the polar inorganic subphase. Indeed, the analysis of the luminescence decay profiles of $Ru(bpy)_3^{2+}$ in the presence of MV^{2+} for the present material gave results also shown in Table I. It is now seen that an impressive decrease of the value of *f* takes place which further decreases if we pass from a matrix to a film made by the same surfactant/silica composition. *f* is smaller than the percolation threshold ($f < 2/3$), indicating that the charged probes are confined and restricted, which is expected, because they are not residing in the organic subphase, the only subphase that allows mobility. That mobility is restricted for the charged probes, but allowed for the hydrophobic ones, is also seen by the values *K* in the third column of Table I. *K* values have been calculated with the help of Eq. (6). Eq. (6) gives the evolution of the reaction probability in the course of time. Time 0 is the point when the exciting pulse begins. We have chosen to calculate the reaction probability 700 ns after time-0 point. This is approximately the time range convenient to apply to both pyrene and $Ru(bpy)_3^{2+}$ [30]. It was then found that whereas in the case of pyrene the reaction goes on after 700 ns, in the case of $Ru(bpy)_3^{2+}$ the reaction is terminated (i.e., *K* is practically zero). In other words, in the case of charged probes the reaction is locally restricted and it occurs within a limited period of time, while in the case of mobile probes the reaction goes on by diffusion for a longer period of time. The above analysis then provides very important information about probe localization and mobility inside the nanocomposite material.

Table I. Data Obtained by Time-Resolved Fluorescence (Luminescence) Analysis Using Eqs. (5) and (6), for a Nanocomposite Material Made of Silica and Cetyltrimethylammoniumbromide and Doped with Various Probes*

Molar ratio of quencher/CTAB	*f*	*K* ($10^6 s^{-1}$)
Pyrene excimers		
1/100	0.71	2.1
1/33	0.72	2.6
1/10	0.69	3.5
Pyrene-C153		
1/40000	0.71	1.0
1/10000	0.69	1,7
1/1000	0.69	2,7
$Ru(bpy)_3^{2+} - MV^{2+}$ bulk		
1/33	0.50	0.1
1/20	0.49	0.1
1/5	0.49	0.2
$Ru(bpy)_3^{2+} - MV^{2+}$ film		
1/33	0.23	0.1
1/20	0.25	0.2
1/10	0.28	0.2

* The composition is defined for the precursor sol in moles/litre: 0.8 tetramethoxysilane; 0.1 CTAB; 0.00002 pyrene; 0.001 $Ru(bpy)_3^{2+}$ quencher concentration is expressed as ratio over CTAB concentration in column 1.

(Adapted from Ref. [30].)

Geometrical Parameters Obtained by Resonance-Energy-Transfer Quenching

As already said, luminescence decay profiles, under conditions of resonance energy transfer between practically immobile partners in a restricted domain, can be described by the model of Eq. (3). Such conditions are satisfied for a dispersion of donor–acceptor pairs in a layered film composed of silica and CTAB [27]. It has been shown that nanocomposite films composed of the above components, synthesized through the sol-gel method are structured in alternating layers of silica and surfactant bilayers [27,55,56]. When the hydrophobic pyrene-C153 donor–acceptor pair is dispersed in such a film, it is solubilized at the interface between the surfactant head groups and the silica layer. Pyrene fluorescence is quenched by energy transfer to C153, as already said. Fitting the decay profiles of pyrene in the presence of C153 by Eq. 3 gave the values of the exponent f and the constant C. A series of values of C and f can be obtained by fixing pyrene and varying C153 concentration. An example is given in Table II for the above CTAB/silica films [27]. With the help of the calculated values of C and f and the analytical expressions for C and f given by Eq. (7) geometrical parameters concerning the film can be extracted. The data of Table II suggest that, within experimental error, the value of f is not changing with C153 concentration. Its average measure is 0.46, which indicates, according to the relation $f = d/s$ (Eq. (7)), that $d = 2.8$, under the assumption that energy is transferred by dipole–dipole interaction ($s = 6$). This dimensionality, which is close to 3.0, a value that corresponds to a homogeneous and isotropic medium, is rather high for a two-dimensional distribution of reactants as expected for the present film. This means that excited pyrene can interact with C153 acceptors across the layer, which should then be thinner than the critical reaction radius. Indeed, for the pyrene-C153 pair $R_0 = 34$ Å [54], while the layer thickness given in Ref. [55] is around 10Å for silica and 27Å for the surfactant bilayer. More on this analysis can be found in Ref. [27]. It is obvious that important geometrical information can be extracted on nanocomposite films by applying the stretched-exponential model of Eq. (3).

Table II. Data Obtained by Fitting Eq. (3) to the Fluorescence Decay Profiles of Pyrene in the Presence of C153 Dispersed in a Nanocomposite Film Made of Silica and Cetyltrimethylammoniumbromide*

Molar ratio of C153/CTAB	f	C
1/70	0.48	5.0
1/100	0.48	3.4
1/150	0.45	2.6
1/200	0.44	1.5

* The composition is defined for the precursor sol in moles/litre: 0.8 tetramethoxysilane; 0.21 CTAB; 0.005 pyrene; quencher concentration is expressed as ratio over CTAB concentration in column 1.
(Adapted from Ref. [27].)

CONCLUSIONS

Nanocomposite organic/inorganic materials are complex systems composed of two subphases mixed in the nanoscale. Time-resolved fluorescence analysis can be used to extract indirect information on the structure and the dynamics of these systems. A model of stretched exponentials can fit fluorescence (luminescence) decay profiles and by proper analysis to provide a variety of useful information. This model is valid for any type of fluorophore-quencher interaction, be it by energy-transfer or by diffusion-controlled quenching or both.

REFERENCES

1. A. Stein, B. J. Melde, and R. C. Schroden (2000) Hybrid organic-inorganic mesoporous silicates Nanoscopic reactors coming of age, *Adv. Mater.* **12**, 1403–1419.
2. M. Muller, R. Zentel, T. Maka, S. G. Romanov, and C. M. Sotomayor Torres (2000) Photonic crystal filsm with high refractive index, *Adv. Mater.* **12**, 1499–1503.
3. H.-S. Yun, K. Miyazawa, H. Zhou, I. Honma, and M. Kuwabara (2001) Synthesis of mesoporous thin TiO_2 films with hexagonal pore structures using triblock copolymer templates, *Adv. Mater.* **13**, 1377–1380.
4. H. Miyata and K. Kuroda (2000) Formation of a continuous mesoporous silica film with fully aligned mesochannels on a glass substrate, *Chem. Mater.* **12**, 49–54.
5. P. Kipkemboi, A. Fogden, V. Alfredsson, and K. Flodstrom (2001) Triblock copolymers as templates in mesoporous silica formation: Structural dependence on polymer chain length and synthesis temperature, *Langmuir* **17**, 5398–5402.
6. K. Dahmouche, C. V. Santilli, S. H. Pulcinelli, and A. F. Craievich (1999) Small-angle X-ray scattering study of sol-gel-derived siloxane-PEG and siloxane-PPG hybrid materials, *J. Phys. Chem. B* **103**, 4937–4942.
7. M. E. Brik, J. J. Titman, J. P. Bayle, and P. Judeinstein (1996) Mapping of motional heterogeneity of organic-inorganic nanocomposite gels, *J. Polym. Sci.* **34**, 2533–2542.
8. N. Groselj, M. Gaberscek, U. Opara-Krasovec, B. Orel, G. Drazic, and P. Judeinstein (1999) Electrical and IR spectroscopic studies of peroxopolytungstic acid/organic-inorganic hybrid gels, *Solid State Ionics* **125**, 125–133.
9. K. Nishio, K. Okubo, Y. Watanabe, and T. Tsuchiya (2000) Structural analysis and properties of organic-inorganic hybrid ionic conductor prepared by the sol-gel process, *J. Sol-Gel. Sci. Technol.* **19**, 187–191.
10. E. Shouji and D. A. Buttry (1999) New organic-inorganic nanocomposite materials for energy storage applications, *Langmuir* **15**, 669–673.
11. L. M. Ilharco and J. M. G. Martinho (1999) Hybrid and nonhybrid silica sol-gel systems doped with 1,12-bis(1-pyrenyl)dodecane, *Langmuir* **15**, 7490–7494.

12. J. Wu, M. M. Abu-Omar and S. H. Tolbert (2001) Fluorescent probes of the molecular environment within mesostructured silica/surfactant composites under high pressure, *Nanoletters* **1**, 27–31.
13. C. Sanchez, F. Ribot, and B. Lebeau (1999) Molecular design of hybrid organic-inorganic nanocomposites synthesized via sol-gel chemistry, *J. Mater. Chem.* **9**, 35–44.
14. L. D. Carlos, V. deZea Bermudez, R. A. S. Ferreira, L. Marques and M. Assuncao (1999) Sol-gel derived urea-cross-linked organically modified silicates: 2. Blue-light emission, *Chem. Mater.* **11**, 581–588.
15. D. Segal (1989) *Chemical Synthesis of Advanced Ceramic Materials*, Cambridge University Press, Cambridge.
16. L. L. Hench and J. K. West (1990) The sol-gel process, *Chem. Rev.* **90**, 33–72.
17. R. A. Caruso, M. Antonietti, M. Giersig, H.-P. Hentze, and J. Jia (2001) Modification of TiO_2 network structures using a polymer gel coating technique, *Chem. Mater.* **13**, 1114–1123.
18. Y. Natsume and H. Sakata (2000) Zinc oxide films prepared by the sol-gel spin coating, *Thin Solid Films* **372**, 30–36.
19. E. Yariv and R. Reisfeld (1999) Laser properties of pyrromethene dyes in sol-gel glasses, *Optical Mater.* **13**, 49–54.
20. F. del Monte, M. L. Ferrer, and D. Levy (2001) Probing the chemical environment at the porous cage of ormosils through the fluorescence of oxazine 1, *J. Mater. Chem.* **11**, 1745–1751.
21. R. B. Bhatia, C. J. Brinker, A. K. Gupta, and A. K. Singh (2000) Aqueous sol-gel process for protein encapsulation, *Chem. Mater.* **12**, 2434–2441.
22. C. Rottman, G. Grader, Y. De Hazan, S. Melchior, and D. Avnir (1999) Surfactant-induced modification of dopants reactivity in sol-gel matrices, *J. Am. Chem. Soc.* **121**, 8533–8543.
23. P. Yang, D. Zhao, D. I. Margolese, B. F. Chmelka, and G. D. Stucky (1999) Block copolymer templating syntheses of mesoporous metal oxides with large ordering lengths and semicrystalline framework, *Chem. Mater.* **11**, 2813–2826.
24. P. Schmidt-Winkel, C. J. Glinka, and G. D. Stucky (2000) Microemulsion templates for mesoporous silica, *Langmuir* **16**, 356–361.
25. D. H. W. Hubert, M. Jung, and A. L. German (2000) Vesicle templating, *Adv. Mater.* **12**, 1291–1294.
26. V. Antochshuk and M. Jaroniec (2000) Functionalized mesoporous materials obtained via interfacial reactions in self-assembled silica-surfactant systems, *Chem. Mater.* **12**, 2496–2501.
27. M. Ferrer and P. Lianos (1996) Study of silica-surfactant composite films with fluorescent probes, *Langmuir* **12**, 5620–5624.
28. V. Bekiari, M. Ferrer, S. Stathatos, and P. Lianos (1998) Fluorescence probing of composite organic/inorganic transparent matrices, *J. Sol-Gel. Sci. Technol.* **13**, 95–98.
29. M-L. Ferrer, V. Bekiari, P. Lianos, and D. Tsiourvas (1997) Leaching of organic molecules from composite silica/surfactant films into water, *Chem. Mater.* **9**, 2652–2658.
30. V. Bekiari, M.-L. Ferrer, and P. Lianos (1999) Time-resolved fluorescence quenching studies in nanocomposite materials made of silica and cetyltrimethylammonium bromide, *J. Phys. Chem. B.* **103**, 9085–9089.
31. E. Stathatos, P. Lianos, and Ch. Krontiras (2001) Dye-sensitized photoelectrochemical cell using a nanocomposite SiO_2/poly(ethylene glycol) thin film as electrolyte support. Characterization by time-resolved luminescence and conductivity measurements, *J. Phys. Chem. B.* **105**, 3486–3492.
32. M. Schneider and K. Mullen (2000) Hybrid materials doped with covalently bound perylene dyes through the sol-gel process, *Chem. Mater.* **12**, 352–362.
33. A. O. Ribeiro, J. C. Biazzoto, and O. A. Serra (2000) A phthalocyanine covalently bonded to a silica network by a sol-gel process, *J. Non-cryst. Solids* **273**, 198–202.
34. F. Ben, B. Boury, R. J. P. Corriu, and V. Le Strat (2000) Evidence of an organization of nanostructured silica-based hybrid materials prepared by sol-gel polymerization, *Chem. Mater.* **12**, 3249.
35. Y. Chen and J. O. Iroh (1999) Synthesis and characterization of polyimide/silica hybrid composites, *Chem. Mater.* **11**, 1218–1222.
36. P. Innocenzi, G. Brusatin, M. Guglielmi, and R. Bertani (1999) New synthetic route to (3-glycidoxypropyl)trimethoxysilane-based hybrid organic-inorganic materials, *Chem. Mater.* **11**, 1672–1679.
37. T. Dantas de Morais, F. Chaput, J.-P. Boilot, K. Lahlil, B. Darracq, and Y. Levy (2000) Organic electroluminescence, *C. R. Acad. Sci. Paris* **1-IV**, 479–491.
38. E. Stathatos, P. Lianos, U. Lavrencic Stangar, B. Orel and P. Judeinstein (2000) Structural study of hybrid organic/inorganic polymer gels using time-resolved fluorescence probing, *Langmuir* **16**, 8672–8676.
39. V. Bekiari, P. Lianos, U. Lavrencic Stangar, B. Orel and P. Judeinstein (2000) Optimization of the intensity of luminescence emission from silica/poly(ethylene oxide) and silica/poly(propylene oxide) nanocomposite gels, *Chem. Mater.* **12**, 3095–3099.
40. V. Bekiari, E. Stathatos, P. Lianos, U. Lavrencic Stangar, B. Orel and P. Judeinstein (2001) Studies on hybrid organic/inorganic nanocomposite gels using photoluminescence techniques, *Chem. Month.* **132**, 97–102.
41. E. Stathatos, P. Lianos, U. Lavrencic Stangar, and B. Orel (2001) Study of laser action of coumarine-153 incorporated in sol-gel made silica/poly(propylene oxide) nanocomposite gels, *Chem. Physics Lett.* **345**, 381–385.
42. J. R. Lakowicz (1983) *Principles of Fluorescence Spectroscopy*, Plenum Press, New York.
43. A. Blumen, (1981) Excitation transfer from a donor to acceptors in condensed media: a unified approach, *Nuovo Cimento* **63B**, 50–58.
44. A. Blumen and J. Manz (1979) On the concentration and time-dependence of the energy transfer to randomly distributed acceptors, *J. Chem. Phys.* **71**, 4694–4702.
45. J. Klafter and A. Blumen (1984) Fractal behavior in trapping and reaction, *J. Chem. Phys.* **80**, 875–877.
46. A. Blumen, J. Klafter, and G. Zumofen (1986) in Models for reaction dynamics in glasses, *Optical Spectroscopy of Glasses*, I. Zschokke! (ed.), D. Reidel, p. 199–265.
47. P. Lianos and P. Argyrakis (1994) $A+B\rightarrow B$ reaction for unequal reactant concentrations, *J. Phys. Chem.* **98**, 7278–7283.
48. P. Lianos (1996) Time-resolved fluorescence quenching models in restricted geometries, *Heter. Chem. Rev.* **3**, 53–63.
49. P. Levitz, J. M. Drake, and J. Klafter (1988) Critical evaluation of the application of direct energy transfer in probing the morphology of porous solids, *J. Chem. Phys.* **89**, 5224–5236.
50. K. Nakashima, Y. S. Liu, P. Zhang, J. Duhamel, J. Feng, and M. A. Winnik (1993) Picosecond fluorescence studies of energy transfer on the surface of poly(butyl methacrylate) latex particles, *Langmuir* **9**, 2825–2831.
51. R. Rammal and G. Toulouse (1983) Random walks on fractal structures and percolation clusters, *J. Physique-Lett.* **44**, 13–22.
52. P. W. Klymko and R. Kopelman (1983) Fractal reaction kinetics: Exciton fusion on clusters, *J. Phys. Chem.* **87**, 4565–4567.
53. M. S. Mendiola and G. C. Farrington (1992) Conductivities and viscosities of polyethylene glycol (PEG) electrolytes containing divalent metal bromides, *Solid State Ionics* **53–56**, 1059–1063.
54. P. J. Tummino and A. Gafni (1993) Determination of the aggregation number of detergent micelles using steady-state fluorescence quenching, *Biophys. J.* **64**, 1580–1587.
55. M. Ogawa (1994) Formation of novel oriented transparent films of layered silica-surfactant nanocomposites, *J. Am. Chem. Soc.* **116**, 7941–7942.
56. M. Ogawa (1995) Incorporation of pyrene into an oriented transparent film of layered silica-hexadecyltrimethylammonium bromide nanocomposite, *Langmuir* **11**, 4639–4641.